TOUGHREACT: A Simulation Program for Non-isothermal Multiphase Reactive Geochemical Transport in Variably Saturated Geologic Media

Tianfu Xu, Eric Sonnenthal, Nicolas Spycher and Karsten Pruess

Earth Sciences Division, Lawrence Berkeley National Laboratory
University of California, Berkeley, CA 94720, USA

Abstract. TOUGHREACT is a numerical simulation program for chemically reactive non-isothermal flows of multiphase fluids in porous and fractured media. The program was written in Fortran 77 and developed by introducing reactive geochemistry into the multiphase fluid and heat flow simulator TOUGH2. A variety of subsurface thermo-physical-chemical processes are considered under a wide range of conditions of pressure, temperature, water saturation, ionic strength, and pH and Eh. Interactions between mineral assemblages and fluids can occur under local equilibrium or kinetic rates. The gas phase can be chemically active. Precipitation and dissolution reactions can change formation porosity and permeability. The program can be applied to many geologic systems and environmental problems, including geothermal systems, diagenetic and weathering processes, subsurface waste disposal, acid mine drainage remediation, contaminant transport, and groundwater quality. Here we present two examples to illustrate applicability of the program: (1) injectivity effects of mineral scaling in a fractured geothermal reservoir and (2) CO_2 disposal in a deep saline aquifer.

Key words: Reactive fluid flow, Geochemical transport, TOUGHREACT, Hydrothermal systems, Mineral scaling, Clay swelling, Injectivity enhancement, CO_2 geologic sequestration, Saline aquifer.

1. Introduction

Coupled modeling of subsurface multiphase fluid and heat flow, solute transport, and chemical reactions can be applied to many geologic systems and environmental problems, including geothermal systems, diagenetic and weathering processes, subsurface waste disposal, acid mine drainage remediation, contaminant transport, and groundwater quality. TOUGHREACT is a numerical simulation program for reactive chemical transport that has been developed by introducing geochemistry into the existing framework of a non-isothermal multi-component fluid and heat flow simulator TOUGH2 (Pruess, et al., 1999). A broad range of subsurface thermo-physical-chemical processes are considered under various thermohydrological and geochemical conditions of pressure, temperature, water saturation, ionic strength, and pH and Eh. TOUGHREACT can be applied to one-, two- or three-dimensional porous and fractured media with physical and chemical heterogeneity. The code can accommodate any number of chemical species present in liquid, gas and solid phases. A variety of equilibrium chemical reactions are considered, such as aqueous complexation, gas dissolution/exsolution, and cation exchange. Mineral dissolution/precipitation can take place subject to either local equilibrium or kinetic controls, with coupling to changes in porosity and permeability and capillary pressure in unsaturated systems. Chemical components can also be treated by linear adsorption and radioactive decay.

The TOUGHREACT program is distributed to the public through the US Department of Energy's Energy Science and Technology Software Center (email: estsc@adonis.osti.gov; WorldWideWeb: http://www.osti.gov/estsc/). The distribution CD provides a README file, the source codes and input data files, and a comprehensive user's guide that includes sample problems addressing geothermal reservoirs and hydrothermal systems, nuclear waste isolation, groundwater quality, sequestration of carbon dioxide in saline aquifers, and supergene copper enrichment. Additional information is available on the TOUGH2 homepage, at http://www-esd.lbl.gov/TOUGH2/. The program makes use of "self-documenting" features. The input files for sample problems provide benchmarks for proper code installation, serve as

a self-teaching tutorial in the use of TOUGHREACT, and provide templates to help jump-start new applications.

TOUGHREACT is written in FORTRAN 77. It has been tested on various computer platforms, including Microsoft Windows- and Linux-based PCs, SUN Ultrasparc systems, Compaq Alpha-based workstations, Apple Macintosh G4 and G5 computers, and IBM RISC System/6000 workstations. An effort was made to have the TOUGHREACT source code comply with the ANSIX3.9-1978 (FORTRAN 77) standard, and on most machines the code should compile and run without modifications. The computer memory required by TOUGHREACT depends on the problem size such as numbers of grid blocks, aqueous and gaseous species, and minerals. Parameter statements are used in INCLUDE files. More details are given in the TOUGHREACT manual (Xu et al., 2004c).

2. Main Scope

TOUGHREACT is applicable to one-, two-, or three-dimensional geologic domains with physical and chemical heterogeneity and can be applied to a wide range of subsurface conditions. The temperature (T) and pressure (P) range is controlled by the applicable range of the chemical thermodynamic database, and the range of the EOS module employed. For example, the range in the commonly-used database of EQ3/6 (Wolery, 1992) is 0 to 300°C, 1 bar below 100°C, and water saturation pressure above 100°C. Because the equilibrium constants are generally not as sensitive to pressure as to temperature, the program may be applied to pressures of several hundred bars (corresponding to depths of less than a few km). The temperature and pressure range is limited only by the thermodynamic database. Water saturation can vary from completely dry to fully water-saturated. Activity coefficients of charged aqueous species are computed using an extended Debye-Huckel equation and parameters derived by Helgeson et al. (1981). The model can deal with ionic strengths from dilute to moderately saline water (up to 6 molal for an NaCl-dominant solution). TOUGHREACT can cope with any pH and Eh conditions.

3. Major processes

The major processes for fluid and heat flow are: (1) fluid flow in both liquid and gas phases occurs under pressure, viscous, and gravity forces; (2) interactions between flowing phases are represented by characteristic curves (relative permeability and capillary pressure); (3) heat transfer is by conduction and convection, and (4) diffusion of water vapor and non-condensable gases is included. Thermophysical and geochemical properties are calculated as a function of temperature, such as fluid (gas and liquid) density and viscosity, and thermodynamic and kinetic data for mineral-water-gas reactions.

Transport of aqueous and gaseous species by advection and molecular diffusion is considered in both liquid (aqueous) and gas phases. Depending on the computer memory and CPU performance, any number of chemical species in the liquid, gas and solid phases can be accommodated. Aqueous complexation, acid-base, redox, gas dissolution/exsolution, and cation exchange are considered under the local equilibrium assumption. Mineral dissolution and precipitation can proceed either subject to local equilibrium or kinetic conditions. Linear adsorption and decay can be included.

Changes in porosity and permeability due to mineral dissolution and precipitation can modify fluid flow. This feedback between flow and chemistry can be important and can be considered in our model, but computational work increases if this is modeled. Alternatively, the model can monitor changes in porosity and permeability during the simulation from changes in mineral volume fractions without feedback to the fluid flow. Changes in porosity during the simulation are calculated from changes in mineral volume fractions. Several alternative models for the porosity-permeability relationship are included. Permeability and porosity changes will likely result in modifications to the unsaturated flow properties of the rock, which can be treated by modification of the capillary pressure function using the Leverett scaling relation (Slider, 1976).

4. Solution Method

The flow and transport in geologic media are based on space discretization by means of integral finite differences (IFD; Narasimhan and Witherspoon, 1976). The IFD method gives a flexible discretization for geologic media that allows to use irregular

grids, which is well suited for simulation of flow, transport, and fluid-rock interaction in multi-region heterogeneous and fractured rock systems. For regular grid, IFD is equivalent to conventional finite differences. An implicit time-weighting scheme is used for individual components of flow, transport, and kinetic geochemical reaction.

TOUGHREACT uses a sequential iteration approach (SIA) similar to Yeh and Tripathi (1991), Simunek and Suares (1994), and Walter et al. (1994). After solution of the flow equations, the fluid velocities and phase saturations are used for chemical transport simulation. The chemical transport is solved on a component-by-component basis. The resulting concentrations obtained from solving transport equations are substituted into the chemical reaction model. The system of mixed equilibrium-kinetic chemical reaction equations is solved on a grid block-by-grid block basis by Newton-Raphson iteration (Xu et al., 1999a). Optionally, the chemical transport and reactions are solved iteratively until convergence. An automatic time stepping scheme is implemented in TOUGHREACT, which includes an option to recognize "quasi-stationary states" (QSS; Lichtner, 1988) and perform a "large" time step towards the end of a QSS.

As an alternative to the sequential iterative approach, a sequential non-iterative approach (SNIA) may be used, in which the sequence of transport and reaction equations is solved only once (Walter et al., 1994; Steefel and MacQuarrie, 1996; and Xu et al., 1999b). Xu et al. (1999b) analyzed the accuracy of SIA and SNIA using several test cases. They concluded that the accuracy of SNIA depends mainly on the Courant number, which is defined as $C = v\Delta t/\Delta x$, where v is fluid pore velocity, Δt is time step, and Δx is grid spacing. For small Courant numbers, satisfying the stability condition $C \leq 1$, the differences between SNIA and SIA are generally small. The accuracy of SNIA also depends on the type of chemical process. Therefore, the applicability of the decoupling of chemical reactions from transport will depend on time and space discretization parameters, the nature of the chemical reactions and the desired accuracy. When SNIA is used, the Courant number condition $C \leq 1$ can be automatically enforced during the simulation.

When analyzing water flow through partially saturated porous media, the gas phase may often be considered a passive by stander and need not be represented explicitly (Richards, 1931). This means that for the purpose of solving for water flow, the

entire gas phase is at the same pressure (usually the atmospheric pressure). TOUGHREACT allows a choice of considering saturated-unsaturated liquid phase flow in which only molecular diffusion is considered for gaseous species transport. Alternatively, the full non-isothermal multiphase flow equations (liquid, gas, and heat) may be solved. To test the passive gas phase approach under ambient conditions, Xu et al. (2000) performed numerical simulation experiments on pyrite oxidation in a variably saturated porous medium. They found that under ambient conditions the effects of partial pressure reduction due to oxygen consumption on the fluid flow is not significant, and oxygen diffusion is the dominant gas phase transport process. However, when fluid flow and chemical reactions are strongly coupled, as e.g. in boiling hydrothermal reservoirs, gas phase advection could be essential (White, 1995).

5. Applications

The TOUGHREACT code was extensively verified against analytical solutions and other numerical simulators (Xu and Pruess, 1998; Xu et al., 1999a; Xu and Pruess, 2001b). TOUGHREACT has been applied to a wide variety of problems, some of which are included as examples, such as:

(1) Supergene copper enrichment (Xu et al., 2001).

(2) Mineral alteration in hydrothermal systems (Xu and Pruess, 2001a; Xu et al., 2004a; Dobson et al., 2004; Kiryukhin et al., 2004; Todaka et al., 2004).

(3) Mineral trapping for CO_2 disposal in deep saline aquifers (Xu et al., 2003a and 2004b).

(4) Coupled thermal, hydrological, and chemical processes in boiling unsaturated tuff for the proposed nuclear waste disposal site at Yucca Mountain, Nevada (Sonnenthal and Spycher, 2000; Spycher et al., 2003; Xu et al., 2001).

(5) Modeling of mineral precipitation/dissolution in plug-flow and fracture-flow experiments under boiling conditions (Dobson et al., 2003).

(6) Calcite precipitation in the vadose zone as a function of net infiltration (Xu et al., 2003b).

(7) Stable isotope fractionation in unsaturated zone pore water and vapor (Singleton et al., 2004).

(8) Coupled processes of fluid flow, solute transport, and geochemical reactions in reactive barriers (Kim et al., 2004).

Here we give two illustrative examples of TOUGHREACT applications: (1) mineral scaling during wastewater injection into a fractured geothermal reservoir and (2) CO_2 disposal in a deep saline aquifer.

5.1 Injectivity effects of mineral scaling in a fractured geothermal reservoir

Problem statement

A major concern in the development of hot dry rock (HDR) and hot fractured rock (HFR) reservoirs is achieving and maintaining adequate injectivity, while avoiding the development of preferential short-circuiting flow paths such as those caused by thermally-induced stress cracking. Past analyses of HDR and HFR reservoirs have tended to focus primarily on the coupling between hydrology (flow), heat transfer, and rock mechanics. Recent chemistry studies suggest that rock-fluid interactions and associated mineral dissolution and precipitation effects could have a major impact on the long-term performance of HFR reservoirs (Jacquot, 2000; Durst, 2002; and Bächler, 2003). The present paper uses recent European studies as a starting point to explore chemically-induced effects of fluid circulation in HFR systems. We examine ways in which the chemical composition of reinjected waters can be modified to improve reservoir performance by maintaining or even enhancing injectivity. Chemical manipulations considered here include pH modification and dilution with fresh water. We performed coupled thermo-hydrologic-chemical simulations in which the fractured medium was represented by a one-dimensional MINC model (multiple interacting continua; Pruess and Narasimhan, 1985), using the non-isothermal multi-phase reactive geochemical transport code TOUGHREACT.

Problem setup

Mineralogical conditions

We consider three different mineral assemblages (Table 1). The first represents strongly altered minerals from a highly fractured vein, minerals from the original granite (mainly quartz) that are fully cemented by clays, carbonates, and secondary quartz veins. The second assemblage is composed of altered granite blocks partly cemented by alteration products that consist essentially of clay minerals and carbonates, and is the most porous. The third is the unaltered granite in which the fracture density is close to zero.

Table 1. Initial mineralogical composition of the three zones used in the simulations. Data were taken from Jacquot (2000), Durst (2002), and Bächler (2003). Only the total amount of smectite was reported originally. In the present simulations, Na- and Ca-smectite were distinguished and their volume percentages were assigned with 77 and 23% for Na- and Ca-smectite, respectively, according to the portion of Na^+ and Ca^{+2} charges in water chemical composition (Table 4).

Mineral	Volume percentage of solid rock		
	Fractured vein Alteration	Altered granite	Unaltered granite
Quartz	43.9	4.09	24.2
K-feldspar		13.9	23.6
Plagioclase			42.5
Biotite			4.2
Hornblende			3.1
Chlorite		4.8	2
Calcite	4.3	3.3	0.3
Dolomite	0.7	0.8	
Illite	40.2	24.6	
Na-smectite	7.392	7.469	
Ca-smectite	2.208	2.231	
Pyrite	1	0.7	
Galena	0.3	1.3	
Other minerals (not reactive)		36.81	0.1

Mineral dissolution and precipitation are controlled by kinetics. The parameters in the kinetic rate expression (Appendix A) are shown in Table 2. Only a single kinetic

mechanism was used in this example, acid-catalyzed or neutral. For most minerals, we give two sets of kinetic parameters. A reaction order n (acid-catalyzed) greater than zero is used for mineral dissolution, while n = 0 (neutral) is used for precipitation. For minerals with only one set of the parameters with n = 0, it is used for both dissolution and precipitation.

Table 2. List of kinetic rate parameters used in Eqs. (A.1) and (A.2) for mineral scaling problem (n = 0 for neutral, and n > 0 for acid-catalyzed mechanism)

Mineral	k_{25} (moles m^{-2}s^{-1})	E_a (KJ/mol)	n	Surface area (cm^2/g)
calcite	6.4565×10^{-7}	62.76	0	9.8
	6.9183×10^{-2}	18.98	1	9.8
quartz	1.2589×10^{-14}	87.50	0	9.8
K-feldspar	1.0000×10^{-12}	57.78	0	9.8
	3.5481×10^{-10}	51.83	0.4	9.8
dolomite	1.2589×10^{-9}	62.76	0	9.8
	1.0233×10^{-3}	20.90	0.9	9.8
Na-smectite	1.0000×10^{-13}	62.76	0	151.6
	4.3652×10^{-12}	62.76	0.17	151.6
Ca-smectite	1.0000×10^{-13}	62.76	0	151.6
	4.3652×10^{-12}	62.76	0.17	151.6
illite	1.0000×10^{-13}	62.76	0	151.6
	4.3652×10^{-12}	62.76	0.17	151.6
pyrite	4.0000×10^{-11}	62.76	0	12.9
galena	4.0000×10^{-11}	62.76	0	12.9
chlorite	2.5119×10^{-12}	62.76	0	9.8

Geometric configuration and fluid flow parameters

A one-dimensional MINC (multiple interacting continua) model was used (Figure 1). Subgrid 1 represents the fracture vein alteration. Subgrids 2 and 3 represent the altered and unaltered granite, respectively. The MINC method can resolve "global" flow and diffusion of chemicals in the fractured rock and its interaction with "local" exchange between fractures and matrix. Details on the MINC method for reactive geochemical transport are described by Xu and Pruess (2001b).

We consider an idealized fractured porous medium with two perpendicular sets of planar, parallel fractures of equal aperture and spacing. Because of the assumed symmetry only one column of matrix blocks needs to be modeled. Our conceptual model considers a one-dimensional flow tube between injection and production well, which

9

should be considered as a small sub-volume of a much more extensive 3-D reservoir. From the injection side to the production side, the model consists of 72 grid blocks representing 600 m distance. The block size gradually increases from 0.1 m at the injection side to 20 m at the production side.
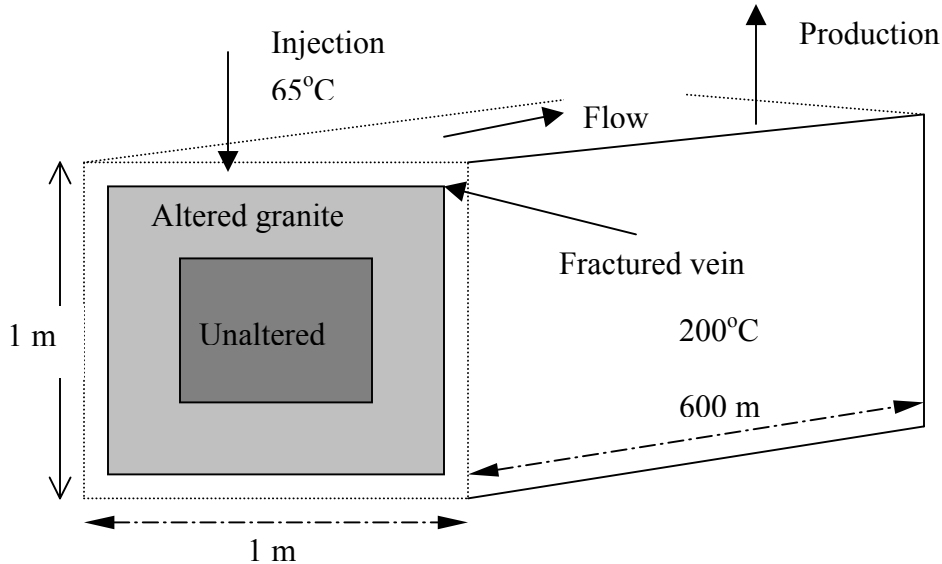
Figure 1. Subgridding in the "multiple interacting continua" (MINC) method. The figure represents a view of a rock matrix column that is bounded by fractures.

Hydrological parameters used in the present simulations are listed in Table 3. Notice that some are different from those of Durst (2002) and Bächler (2003). For example, previous investigators used a permeability of 1×10^{-11} m^2 and a porosity of 0.1 for the fractured vein. The objective of the present study is to explore methods for minimizing mineral scaling and clay swelling, mitigating injection water chemistry, and preserving or enhancing injectivity.

Even though we took some data from the European HDR site as a starting point, we attempted to use thermophysical conditions and parameters that could represent general geothermal reservoirs. Initial reservoir temperature and pressure were 200°C and 50 MPa, respectively. An over-pressure of 2 MPa was applied to the injection (left) side. Injected water temperature was taken as 65°C. Conductive heat exchange with the surrounding low- permeability rock is an important process, and is treated with a semi-analytical technique developed by Vinsome and Westerveld (1980). In the present

simulations, chemical interactions in the unaltered granite zone were not considered. This does not significantly affect chemical changes in the fractured vein because of the extremely low permeability of the granite.

Table 3. Hydrogeologic and thermal parameters used for the three mineralogical zones (a density of 2650 kg.m^{-3}, a heat capacity of 1000 J.kg^{-1} K^{-1}, and a diffusivity of 1×10^{-9} m^2.s^{-1} were used for all three zones).

Parameters	fractured vein	altered granite	unaltered granite
Volume fraction	10%	60%	30%
Permeability (m^2)	2×10^{-12}	2×10^{-15}	2×10^{-18}
Porosity	0.2	0.1	0.02
Thermal conductivity (W.m^{-1} K^{-1})	2.9	3	3
Tortuosity	0.3	0.1	0.05

Water chemistry

We started with a 165°C water sample taken from Soultz Well CPK1 at 3500 m depth (Table 4). Initial water chemical compositions for the fractured vein and altered granite zones were obtained by equilibrating the sample water with their corresponding mineral compositions (Table 2) at a temperature of 200°C.

Four types of injection waters with different chemical compositions were considered in the present simulations (Table 5). The injectate composition was not allowed to change over time. The first type corresponded to the native water in the fractured vein zone but with a lower temperature of 65°C, which should be close to the produced reservoir wastewater without surface treatment. To understand the effects of clay (smectite and illite) swelling, we then used an injection water (Water 2) obtained by diluting Water 1 by a factor of 5 (i.e., one unit of reservoir water mixed with four units of fresh water). To avoid the scaling and possibly enhance porosity and permeability, we maintained a pH of 7 by adding alkali to Water 1 and allowed sufficient time to precipitate minerals out (mainly calcite and quartz). The resulting composition is listed as Water 3 in Table 5. Water 4 was obtained by diluting Water 1 by a factor of 2 (mixing one unit of reservoir water with one unit of fresh water), and then using the same titration procedure as for Water 3.

11

Table 4. Initial water chemical compositions (mol/l) used in the simulations. The composition given in the second column was from a Soultz Well GPK1 sample (Durst, 2002). No measurements for Fe, Al, and Pb concentrations in the sample were reported, and small values were assumed for consistency because of the presence of minerals with these components.

		Fractured vein	Altered granite
Chemical components	Soultz Well GPK1 at 3500 depth (165°C)	Equilibrium with the minerals at 200°C	Equilibrium with the minerals at 200°C
Ca	1.820×10^{-1}	1.810×10^{-1}	1.706×10^{-1}
Mg	4.610×10^{-3}	5.874×10^{-3}	5.540×10^{-3}
Na	1.213	1.213	1.212
K	7.180×10^{-2}	7.179×10^{-2}	9.439×10^{-2}
Fe	1.491×10^{-6}	2.191×10^{-5}	1.996×10^{-7}
Cl	1.72	1.72	1.72
SiO$_2$(aq)	3.500×10^{-3}	4.129×10^{-3}	4.131×10^{-3}
HCO$_3$	7.500×10^{-3}	7.795×10^{-3}	1.727×10^{-3}
SO$_4$	2.020×10^{-3}	2.062×10^{-3}	2.392×10^{-3}
Al	5.656×10^{-9}	5.655×10^{-9}	$1.518E\times10^{-6}$
Pb	1.000×10^{-12}	1.296×10^{-6}	3.391×10^{-8}
pH	5.03	5.55	5.92
I (ionic strength)	1.8834	1.8877	1.8721

Table 5. List of types of injection waters with different chemical compositions (mol/l) at 65°C temperature used in the simulations.

Injection water	Water 1	Water 2	Water 3	Water 4
Chemical component	Initial fractured vein water (with different T)	Diluting Water 1 by a factor of 5	Equilibrating Water 1 with fractured vein mineralogy at 65°C and pH=7	Diluting Water 1 by a factor of 2, followed by the same titration procedure as Water 3.
Ca	1.810×10^{-1}	3.620×10^{-2}	1.715×10^{-1}	8.587×10^{-2}
Mg	5.874×10^{-3}	1.175×10^{-3}	7.853×10^{-3}	4.010×10^{-3}
Na	1.213	2.426×10^{-1}	1.213	6.065×10^{-1}
K	7.179×10^{-2}	1.436×10^{-2}	7.180×10^{-2}	3.589×10^{-2}
Fe	2.191×10^{-5}	4.382×10^{-6}	1.511×10^{-6}	7.892×10^{-7}
Cl	1.72	3.440×10^{-1}	1.72	8.600×10^{-1}
SiO$_2$(aq)	4.129×10^{-3}	8.258×10^{-4}	5.064×10^{-4}	5.066×10^{-4}
HCO$_3$	7.795×10^{-3}	1.559×10^{-3}	$2.490E\times10^{-4}$	3.419×10^{-4}
SO$_4$	2.062×10^{-3}	4.124×10^{-4}	2.020×10^{-3}	1.010×10^{-3}
Al	5.655×10^{-9}	1.131×10^{-9}	5.209×10^{-10}	1.546×10^{-9}
Pb	1.296×10^{-6}	2.592×10^{-7}	1.342×10^{-10}	1.826×10^{-11}
pH	5.55	5.96	7	7
I (ionic strength)	1.888	0.378	1.865	0.933

Simulation setup

A total of six simulations were performed using different combinations of over-pressure at the injection side, porosity-permeability (ϕ-k) relationship, clay swelling, and injection water chemistry, as summarized in Table 6. In the first simulation an over-pressure of 2 MPa, a simple cubic Kozeny-Carman ϕ-k relationship (Eq. C.1 in Appendix C), and injection Water 1 (the "base case") was used. To demonstrate the effect of higher over-pressure on injectivity, Simulation 2 used a value of 5 MPa. Other conditions and parameters were not changed from the base case. We called this the "over-pressure simulation".

Simulation 3 used the Verma and Pruess (1988) ϕ-k relationship of Eq. C.2 in Appendix C ("Verma-Pruess simulation"). This relationship requires two parameters, one is the "critical" porosity ϕ_c at which permeability is reduced to zero, and another is n, a power law exponent. In the present simulations, we simply used a ϕ_c of 0.16 (80% of initial porosity of 0.2 for the fractured vein), and an n of 2. A ϕ_c of 80% initial porosity is quite reasonable and may be conservative. A permeability experiment of Moore et al. (1983), in which a heated aqueous fluid was passed down a temperature gradient through Westerly Granite, showed a reduction in permeability of 96% with an 8% reduction of the initial porosity over a two-week period.

Simulation 4 used Water 2 (one unit of reservoir water with four units of fresh water). The native reservoir water has an ionic strength (I) equal to 1.8834, the diluted injection water has an I of 0.37755. The minimum ionic strength I_{min} (Eq. B.2 in Appendix B) to maintain clay density is dependent on the type of clays, type of salts dissolved in water, and temperature and pressure conditions. In the present simulations, we simply select I_{min} = 1.5, which is slightly below the I of the native reservoir water. The maximum density reduction factor f_{max} is also a predetermined parameter. In the reservoir, the clay may not be well contacted by the injected water and conditions could be different from the lab. We used a maximum density reduction factor f_{max} = 5%. We called this the "swelling simulation".

Simulation 5 injected Water 3 that was obtained by precipitating minerals out under pH 7 conditions. The purpose is to avoid carbonate scaling and potentially enhance

porosity and permeability by mineral dissolution. We called this simulation the "pH 7" simulation.

Simulation 6 injected Water 4 that is similar to Water 3 but mixed with fresh water (1:1, "mixing simulation"). This water has a I of 0.93315 (below 1.5 of the I_{min}), and slight clay swelling will occur.

Table 6. List of simulations with different combinations of over-pressure, porosity-permeability relationship, clay swelling, and injection water chemistry.

Simulation	Over-pressure at injection	ϕ-k relationship	Clay swelling	Injection water chemistry
1 (base case)	2Mpa	Kozeny-Carman		Water 1 (see Table 5)
2 (over-pressure)	5Mpa	Kozeny-Carman		Water 1
3 (Verma-Pruess)	2Mpa	Verma-Pruess		Water 1
4 (swelling)	2Mpa	Verma-Pruess	f_{max} = 5%	Water 2
5 (pH 7)	2Mpa	Verma-Pruess	f_{max} = 5%	Water 3
6 (mixing)	2Mpa	Verma-Pruess	f_{max} = 5%	Water 4

Results and discussion

The injection rates over time obtained from the six different simulations are presented in Figure 2. By increasing the over-pressure at the injection point from 2 to 5 MPa, the injection rate is proportionally increased initially (compare Simulations 2 and 1). After five years, the temperature at the production side decreases to below 200°C due to the larger injection rate. By using the Verma-Pruess ϕ-k relationship instead of Kozeny-Carman in the base case, the injection rate decreases faster due to a larger permeability reduction (compare Simulations 3 and 1). After ten years, the injection rate declines to 0.016 kg/s from the initial 0.04 kg/s

By considering clay swelling (Simulation 4) using a 1:4 diluted injection water, the injection rate dramatically decreases to 0.01 kg/s in several months. Clay swelling contributes to a porosity decrease of 0.016. Later, decreases in the injection rate occur due to mineral scaling. After five years, the injection rate is close to zero. In actual field operation, the injection would stop before that.

By using pH 7 injection water (Simulation 5) minerals such as calcite have been already precipitated out, the injection rate gradually increases to 0.052 kg/s at ten years

from the initial 0.04 kg/s, which enhances injectivity. At ten years, the temperature at the production side just reaches 200°C due to the enhanced injection rate.

Simulation 6 uses a similar pH 7 injection water as the previous case but diluted 1:1 by mixing with fresh water. This water has an intermediate I of 0.93315 compared to the swelling simulation with I = 0.3776. The clay swelling causes a slight porosity decrease close to 0.01. This reduces the injection rate to about 0.025 from the initial 0.04 kg/s, a reduction that is considerably less than that in Simulation 4 (swelling). Similar to the previous simulation, the diluted pH 7 water also causes dissolution effects and enhances injectivity. The injection rate then increases linearly with time after the clay swelling stops. The rise of permeability is similar to that in Simulation 5. After ten years, the rate reaches about 0.035 kg/s, close to the initial value. This suggests that modifying the injection water could avoid mineral scaling and enhance injectivity. Mitigation is achieved by adding alkali to maintain a higher pH and letting minerals (mainly calcite and quartz) precipitate out prior to reinjection. Further reviewing Figure 2, we can see that injection rates in Simulations 1 and 2 decrease with time and the injection rate vs. time curves have negative slopes even though Simulation 2 applied a much higher over-pressure.
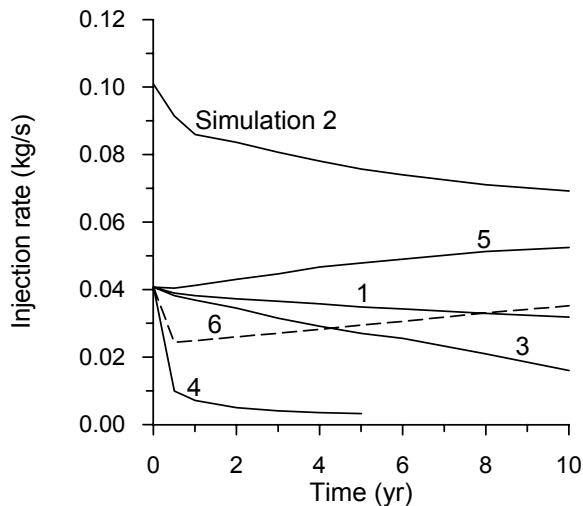
Figure 2. Injection rate (kg/s) over time of the fracture-matrix column with an area of 1 m^2 obtained from different simulations. Simulation 1: base case; 2: over-pressure; 3: Verma-Pruess; 4: swelling; 5: pH 7; 6 mixing.

Changes in porosity are due to mineral dissolution and precipitation, and clay swelling. Porosity increases indicate that mineral dissolution is dominant (Figure 3), while porosity decreases when precipitation dominates. Changes in permeability (Figure 4) are calculated from changes in porosity using Eq. C.1 or C.2 (in Appendix C).

Now let us examine the changes of mineral abundances. For Simulations 1-3, the $65^{o}C$ injection water is over-saturated with quartz and under-saturated with respect to calcite because this water was in equilibrium with reservoir rock at $200^{o}C$. Therefore, quartz is gradually precipitating due to kinetics (Figure 5a). A precipitation peak can be observed because the precipitation rate increases with temperature. Later along the flow path quartz starts to dissolve because as the temperature of the injectate increases quartz tends to be under-saturated again. In reality, the injected water would first precipitate amorphous silica. The use of quartz rather than amorphous silica in the simulation does not affect the results because both minerals have the same chemical composition (SiO_2).

Significant calcite dissolves close to the injection side because calcite solubility decreases with temperature (Figure 6a), which is different from quartz. Calcite has a higher solubility at the injection temperature of $65^{o}C$. As temperatures increase away from the injection point, calcite becomes over-saturated and precipitation occurs. Areas of calcite dissolution and precipitation move gradually away from the injection point due to changes in temperature along the flow path. A maximum of 3.6% volume of calcite has been precipitated after ten years, which is more than one order of magnitude larger than the amount of quartz deposited. Notice that amounts of calcite and quartz precipitation and their distribution depend on their precipitation kinetics.

Dolomite also dissolves close to the injection side but later precipitates. The amounts of dolomite precipitation are about one order of magnitude smaller than calcite. Some pyrite and galena precipitation, and very slight illite and smectite precipitation occur near the injection point.

For the swelling simulation (Simulation 4), precipitation of calcite and quartz is more localized due to the lower injection and the faster temperature increase with distance. For the two pH 7 simulations (Simulations 5 and 6), calcite dissolution occurs constantly throughout the distance and time. The lower temperature ($65^{o}C$) injection water is just saturated in terms of calcite. Along the flow path, temperature increases and

pH decreases (Figure 7a), causing competing effects on calcite solubility. The effect of pH plays a more important role than temperature for calcite, giving rise to calcite dissolution. Quartz also dissolves continually because both higher temperature and lower pH are favorable for quartz dissolution. A maximum of quartz dissolution is close to 2%, which is comparable to calcite dissolution (close to 3%). On the other hand, dolomite precipitation occurs constantly along the flow path and throughout time with a maximum value of 2.3%. Overall dissolution is dominant and porosity increases.

(a) Simulation 1 (Base case)   (b) Simulation 2 (Over-pressure)   (c) Simulation 3 (Verma-Pruess)

(d) Simulation 4 (Swelling)   (e) Simulation 5 (pH 7)   (f) Simulation 6 (Mixing)
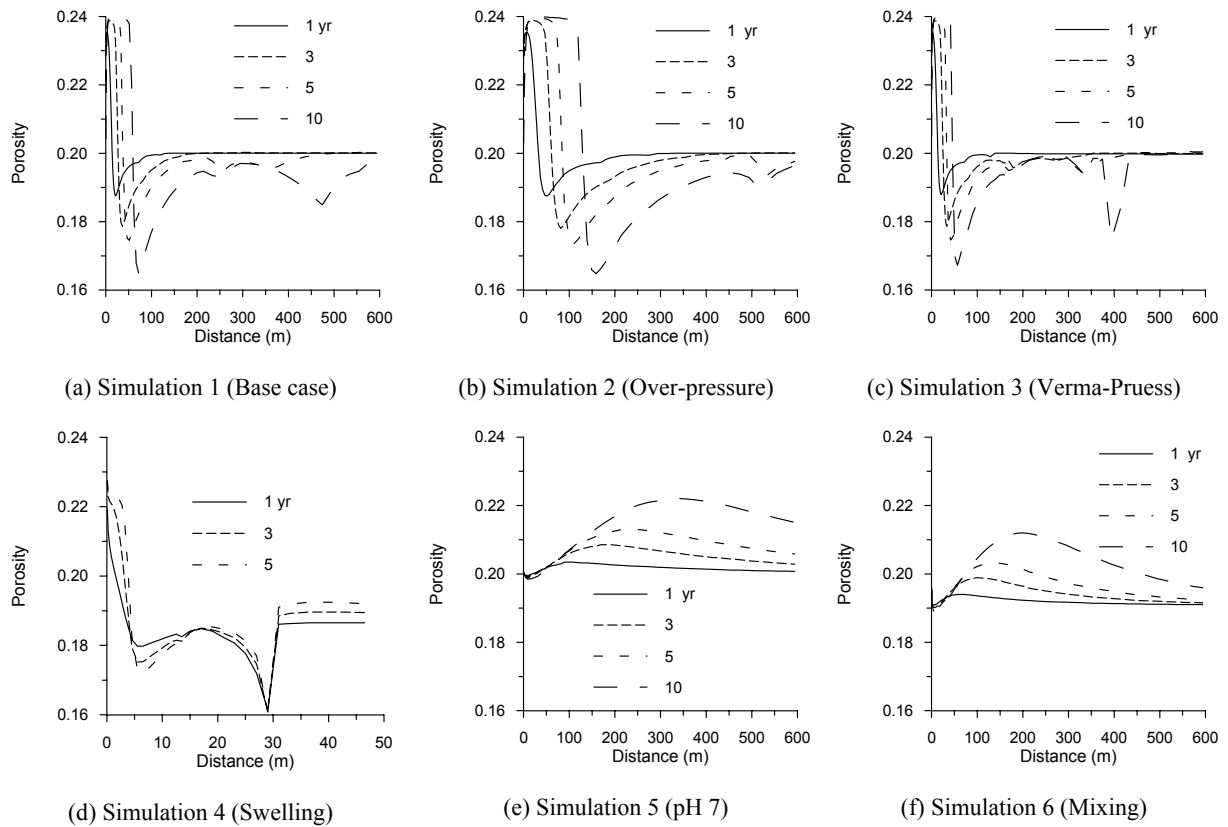
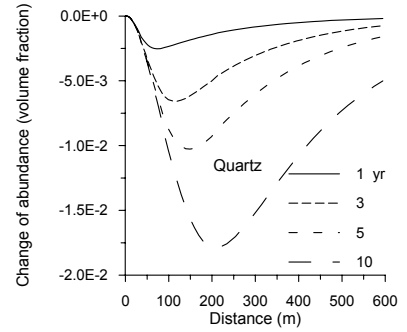**Figure 3.** Distribution of porosity obtained from all six different simulations.
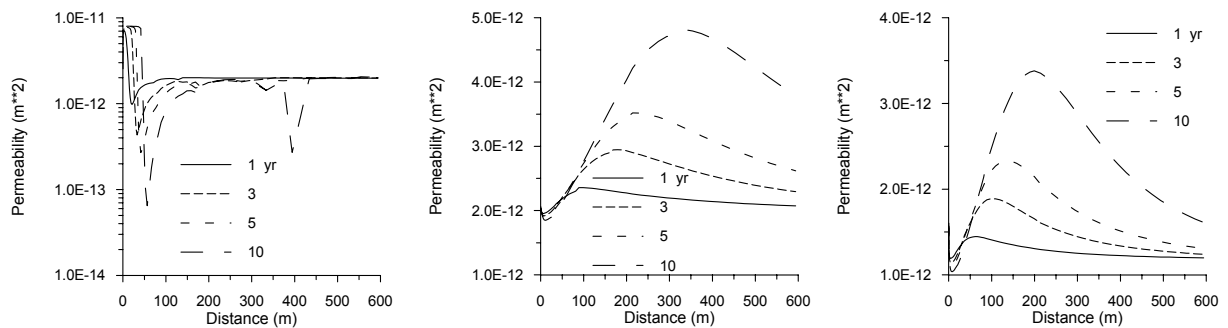
Figure 4. Distribution of permeability obtained from three different simulations.
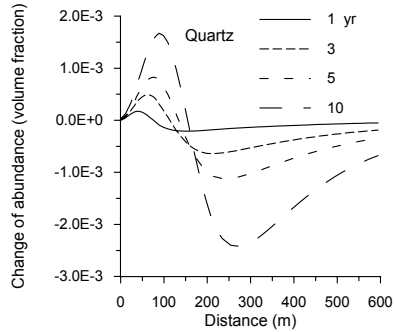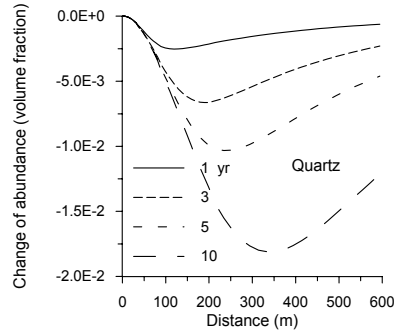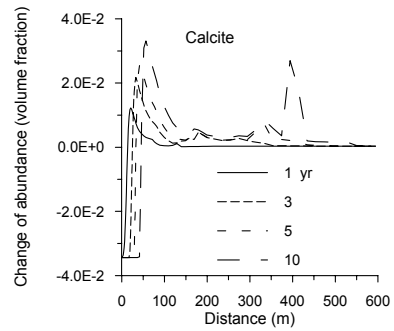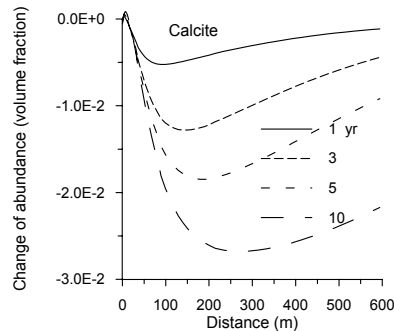

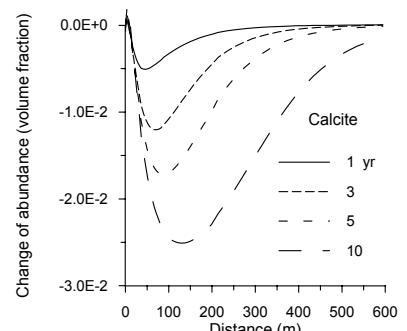(a) Simulation 3 (Verma-Pruess)   (b) Simulation 5 (pH 7)   (c) Simulation 6 (Mixing)

Figure 5. Changes of quartz abundance (given in reservoir volume fractions) obtained from three simulations.

(a) Simulation 3 (Verma-Pruess)   (b) Simulation 5 (pH 7)   (c) Simulation 6 (Mixing)

Figure 6. Changes of calcite abundances (given in reservoir volume fractions) obtained from three simulations.

Now we return to the pH distribution along the flow path (Figure 7a). The higher pH 7 water would eventually displace the lower pH native reservoir water if the rock matrix was not considered in the simulation. The higher H^+ concentration in the matrix diffuses into the fractures, maintaining lower pH. The rock matrix also buffers temperature in the main flow channel at the fracture walls (Figure 7b). If diluted water is injected, the matrix also buffers solute concentrations in the fracture and keeps higher ionic strength (I). However, the buffering capability for I is limited to initial times only, unlike for pH and temperature.
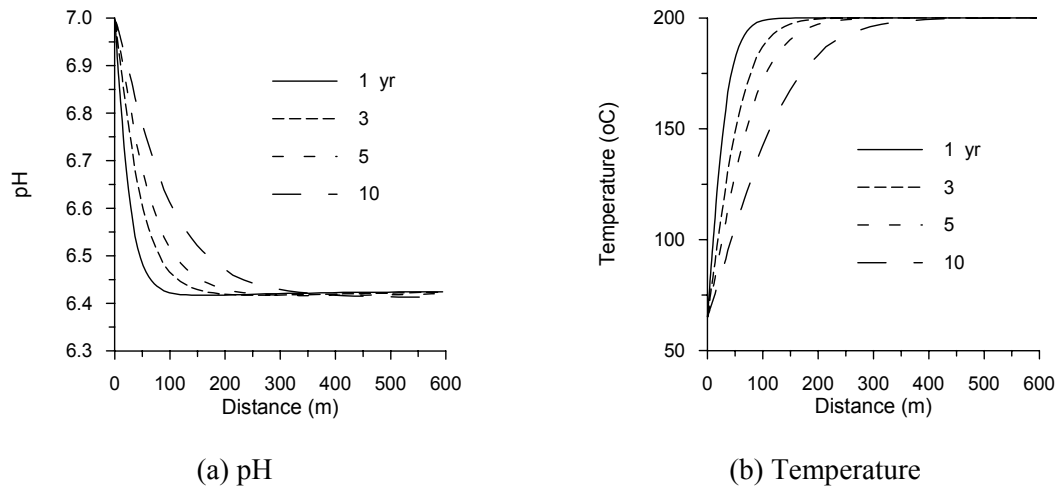
	(a) pH	(b) Temperature

Figure 7. Distribution of pH and temperatures obtained from the mixing simulation (Simulation 6).

Summary

Injecting produced geothermal brines directly back into the reservoir results in mineral scaling (especially calcite). The reinjected highly concentrated water from the geothermal reservoir can maintain clay density without swelling, but this limits the availability of water for injection. Mixing the produced geothermal water with large amounts of fresh water (1:4) can cause serious clay swelling when it is reinjected.

Modifying the injection water could avoid mineral scaling and enhance injectivity. Mitigating injection water chemistry could be an efficient way to achieve this objective. Hydrological approaches such as applying a high over-pressure at the injection well cannot solve the scaling problem. In this work, we added alkali to maintain a higher pH and let minerals (mainly calcite and quartz) precipitate out prior to reinjection. Using this modified injection water results in the injection rate gradually increasing because of continual calcite and quartz dissolution. By mixing the reservoir water with appropriate amounts of fresh water (1:1), together with adding alkali to let minerals precipitate out, clay swelling could be reduced and injectivity be maintained.

The higher pH injection water is not able to simply displace the lower pH native reservoir water because of the buffering effect of the rock matrix. Therefore, the MINC model considering rock matrix subgridding as used in the present simulations is very important for modeling realistically pH and temperature buffering in the fractures.

The reaction kinetics of mineral alteration and the relationship between porosity and permeability changes are uncertain. Sensitivity studies should be performed in the future. The well configuration and data for mineralogical composition in this study were taken from the European HDR research site, but the results and conclusions should be useful for other HFR reservoirs, because calcite and quartz are commonly present in geothermal systems.

Chemical interactions between rocks and fluids will change a HFR reservoir over time, with some changes favorable and others unfavorable. A detailed, quantitative understanding of processes and mechanisms are needed to develop reservoir management tools based on geochemistry. Such novel approach should result in improvements in reservoir performance.

5.2. CO_2 disposal in a deep saline aquifer

Problem statement

The feasibility of storing CO_2 in deep geologic formations has been discussed in the literature over the last decade. Studies include an evaluation of the feasibility of CO_2 aquifer storage in The Netherlands (Lohuis, 1993) and in the Alberta Basin, Canada (Gunter et al., 1997). Furthermore, large-scale CO_2 disposal in an aquifer is already being practiced in the Norwegian sector of the North Sea (Korbol and Kaddour, 1995).

Carbon dioxide is retained in geologic formations in three ways. First, CO_2 can be trapped as a gas or supercritical fluid under a low-permeability caprock. This process, commonly called hydrodynamic trapping, will likely be, in the short term, the most important mechanism of retention. Second, CO_2 can dissolve into the groundwater, referred to as a solubility trapping. The dissolution of CO_2 in groundwater increases the acidity of water and affects the solubilities of minerals composing the host rock matrix. Third, CO_2 can react directly or indirectly with minerals and organic matter in the geologic formation leading to the precipitation of secondary carbonates. The latter process, so-called "mineral trapping", is attractive because it could immobilize CO_2 for long time scales, and prevent its easy return to the atmosphere. The interaction of CO_2 with alkaline aluminosilicate minerals will also result in the formation of dissolved alkali carbonates and bicarbonates, thereby enhancing "solubility trapping".

Numerical modeling of geochemical processes is a necessary tool for investigating the long-term consequences of CO_2 disposal in deep formations (Johnson et al., 2001; McPherson and Lichtner, 2001; White et al., 2001), because alteration of the predominant host rock aluminosilicate minerals is very slow and is not experimentally accessible under ambient deep-aquifer conditions.

During large-scale injection of CO_2 into deep formations, geochemical processes are strongly affected by physical processes such as multiphase fluid flow and solute transport. Fluid pressures will rise as CO_2 displaces formation water in which it partly dissolves. The dissolution of primary and precipitation of secondary minerals change formation porosity and permeability, and could alter fluid flow patterns. All coupled hydrologic and chemical processes affect the feasibility of CO_2 injection and storage in deep formations. Uncoupled batch geochemical modeling and flow simulation are inadequate to describe the complex subsurface physical and chemical interactions expected to occur. A systematic process-based understanding of the coupled physical and chemical phenomena is required.

Definition of test problem

The response of deep formations to CO_2 injection will depend on many factors, including formation permeability and porosity, the presence of heterogeneities such as faults and layers of high or low permeability, the physical and chemical characteristics of the brines, and the nature of the mineral phases that are present. A great deal of specific and detailed information will be required to assess the feasibility of disposing of CO_2 in a brine formation at any particular site, and to develop engineering designs for CO_2 disposal systems. A basic issue in geologic disposal of CO_2 is the physical and chemical behavior in the vicinity of a CO_2 injection well.

Geologic formation

The setup of the problem is similar to that of Xu et al. (2003a), except using the following (1) a porosity of 0.3 instead of 0.1, (2) a temperature of 75ºC (at about 2000 m depth) instead of 40ºC, (3) improved mineralogical composition, and kinetic rate law and parameters.

The geologic formation is assumed to be infinite-acting and homogeneous with a thickness of 100 m, containing 1 M NaCl brine at a constant temperature of 75ºC. Hydrological parameters are given in Table 7. A 1-D radial model is used. This simplification does not consider non-uniform sweep that may occur due to formation heterogeneities, or due to buoyancy forces that would tend to drive CO_2 towards the top of the aquifer. Some justification for a 1-D approach can be derived from the slow rates and long time scales of geochemical changes, which will cause processes to play out over time that will make the distribution of CO_2 more uniform. Initially, injected CO_2 will tend to accumulate and spread out near the top of permeable intervals, partially dissolving in the aqueous phase. CO_2 dissolution causes the aqueous-phase density to increase by a few percent. This will give rise to buoyant convection where waters enriched in CO_2 will tend to migrate downward (Ennis-King and Paterson, 2003). The process of CO_2 dissolution and subsequent aqueous phase convection will tend to mix aqueous CO_2 in the vertical direction. The time scale for significant convective mixing is likely to be slow (of the order of hundreds of years or more; Ennis-King and Paterson, 2003), and may be roughly comparable to time scales for significant geochemical interactions of CO_2.

The well field is modeled as a circular region of 10,000 m radius, at the center of which CO_2 is injected uniformly at a constant rate of 100 kg/s ($\approx$ 8,640 tonnes per day), This injection rate is approximately equivalent to that generated by a 300 MW coal-fired power plant (Hitchon, 1996). A 1-D radial grid was used with a spacing gradually increasing away from the well. The CO_2 injection was assumed to continue for a period of 100 years. The fluid flow and geochemical transport simulation was run for a period of 10,000 years.

Table 7. Hydrogeologic parameters for the radial fluid flow CO_2 disposal problem.

Aquifer thickness	100 m
Permeability	10^{-13} m^2
Porosity	0.30
Compressibility	4.5×10^{-10} Pa^{-1}
Temperature	$75\ ^0C$
Pressure	200 bar
Salinity	0.06 (mass fraction)
CO_2 injection rate	100 kg/s
Relative permeability	
Liquid (van Genuchten, 1980): $$k_{rl} = \sqrt{S^*}\left\{1 - \left(1 - \left[S^*\right]^{1/m}\right)^m\right\}^2$$ irreducible water saturation exponent	$S^* = (S_l - S_{lr})/(1 - S_{lr})$ $S_{lr} = 0.30$ $m = 0.457$
Gas (Corey, 1954): $$k_{rg} = (1 - \hat{S})^2(1 - \hat{S}^2)$$ irreducible gas saturation	$\hat{S} = \dfrac{(S_l - S_{lr})}{(S_l - S_{lr} - S_{gr})}$ $S_{gr} = 0.05$
Capillary pressure	
Van Genuchten (1980) $$P_{cap} = -P_0\left(\left[S^*\right]^{-1/m} - 1\right)^{1-m}$$ irreducible water saturation exponent strength coefficient	$S^* = (S_l - S_{lr})/(1 - S_{lr})$ $S_{lr} = 0.00$ $m = 0.457$ $P_0 = 19.61\,kPa$

Geochemical system

A proxy for sediment from the United States Gulf Coast, modified from that originally presented by Apps (1996), was used for the reactive geochemical transport simulations. The mineralogy is similar to that commonly encountered in sedimentary basins. Apps (1996) presented a batch geochemical simulation of the evolution of Gulf Coast sediments as a basis for interpreting the chemical processes relating to the deep injection disposal of hazardous and industrial wastes.

The initial mineral abundances are shown in Table 8. The specification of formation mineralogy is determined in part by the availability of data. Most studies related to the Tertiary Gulf Coast sediments are concentrated in the state of Texas. The principal reservoir-quality sandstones within that region are respectively, the Frio, the Vicksberg and the Wilcox formations, all of which are found within the lower Tertiary. Of the three formations, the Frio was chosen as a representative candidate for the sequestration of supercritical carbon dioxide. It is the shallowest of the three formations, but over much of its areal extent, it is located at depths between 5,000 and 20,000 ft, sufficient to ensure adequate CO_2 densities for effective storage.

Calcite was assumed to react with aqueous species at local equilibrium because its reaction rate is typically quite rapid. Dissolution and precipitation of other minerals are kinetically-controlled. Kinetic rates are a product of the rate constant and reactive surface area (Eq. A.1 in Appendix A). Multiple mechanisms (including neutral, acid and base) are used for dissolution of minerals (Eqs. A.2 and A.3 in Appendix A). Kinetic parameters: rate constant (k_{25}), the activation energy (E_a), and the power term (n) for each mechanism are listed in Table 8. At any pH the total rate is the sum of the rates via each mechanism. Most of these parameters were taken from Palandri and Kharaka (2004) who compiled and fitted many experimental data reported by a large number of investigators. Parameters for illite were set to those of smectite. Acid pH parameters for siderite, ankerite, and dawsonite were set to those of dolomite. Neutral pH parameters for siderite were taken from Steefel (2001). Neutral pH parameters for ankerite and dawsonite are set to those of siderite.

Precipitation rate data do not exist for most minerals. Several aspects regarding precipitation are different from dissolution, including nucleation, crystal growth and Ostwald ripening processes, as well as the calculation of the reactive surface area (Steefel and van Capellen, 1990). These processes for mineral precipitation are not considered. Parameters for neutral pH in Table 7 were used for precipitation of the corresponding minerals. Notice that different sets of parameters for precipitation can be specified in an input file of the TOUGHREACT program.

The evolution of surface area in natural geologic media is complex, especially for multi-mineralic systems, and is not quantitatively understood at present. Mineral reactive

surface areas (the third column of Table 8) were taken from Sonnenthal and Spycher (2000), which were calculated using a cubic array of truncated spheres that make up the framework of the rock. For clay minerals kaolinite, illite, and smectite, increased surface areas were based on the smaller grain sizes of these sheet silicate minerals (Nagy, 1995). A reactive surface area calculated from grain size may be a poor estimate of the hydrologically accessible mineral surface area. To account for this effect, surface areas listed in Table 8 were reduced by one order of magnitude in the present simulations. The magnitudes of surface areas are highly uncertain and cover a wide range of values. Sensitivity regarding the kinetic rate constants and reactive surface areas should be addressed in the future.

Prior to CO_2 injection, a simulation of water-rock interaction was performed to obtain a nearly equilibrated water chemistry using a pure 1.0 M solution of sodium chloride reacting with the primary minerals listed in Table 8 at a temperature of 75 °C. The resulting water chemistry was used for the initial condition of reactive geochemical transport simulations under CO_2 injection.

Table 8. Initial mineral volume fractions, possible secondary mineral phases, and their kinetic properties. Note that: (1) all rate constants are listed for dissolution; (2) A is the reactive surface area (Eq. A.1 in Appendix A), k_{25} is the kinetic constant at 25°C, E_a is activation energy, and n is the power (Eq. A.3); (3) the power terms n for both acid and base mechanisms are with respect to H^+, (4) for pyrite, the neutral mechanism has a n with respect to $O_2(aq)$, the acid mechanism has two species involved: one n with respect to H^+ and another n with respect to Fe^{3+} (see Eq. A.3); (5) dolomite, Ca-smectite, and pyrite were included in the list of possible secondary mineral phases in the input but they were not formed during the simulation.

| Mineral	Vol.% Of solid	A (cm²/g)	Neutral mechanism		Acid mechanism			Base mechanism		
			k_{25} (mol/m²/s)	E_a (KJ/mol)	k_{25}	E_a	n(H^+)	k_{25}	E_a	n(H^+)
Primary:										
Quartz	57.888	9.8	1.023×10^{-14}	87.7						
Kaolinite	2.015	151.6	6.918×10^{-14}	22.2	4.898×10^{-12}	65.9	0.777	8.913×10^{-18}	17.9	-0.472
Calcite	1.929	Assumed at equilibrium								
Illite	0.954	151.6	1.660×10^{-13}	35	1.047×10^{-11}	23.6	0.34	3.020×10^{-17}	58.9	-0.4
Oligoclase	19.795	9.8	1.445×10^{-12}	69.8	2.138×10^{-10}	65	0.457			
K-feldspar	8.179	9.8	3.890×10^{-13}	38	8.710×10^{-11}	51.7	0.5	6.310×10^{-12}	94.1	-0.823
Na-smectite	3.897	151.6	1.660×10^{-13}	35	1.047×10^{-11}	23.6	0.34	3.020×10^{-17}	58.9	-0.4
Chlorite	4.556	9.8	3.02×10^{-13}	88	7.762×10^{-12}	88	0.5			
Hematite	0.497	12.9	2.512×10^{-15}	66.2	4.074×10^{-10}	66.2	1			
Secondary:										
Magnesite		9.8	4.571×10^{-10}	23.5	4.169×10^{-7}	14.4	1			
Dolomite		9.8	2.951×10^{-8}	52.2	6.457×10^{-4}	36.1	0.5			
Low-albite		9.8	2.754×10^{-13}	69.8	6.918×10^{-11}	65	0.457	2.512×10^{-16}	71	-0.572
Siderite		9.8	1.260×10^{-9}	62.76	6.457×10^{-4}	36.1	0.5			
Ankerite		9.8	1.260×10^{-9}	62.76	6.457×10^{-4}	36.1	0.5			
Dawsonite		9.8	1.260×10^{-9}	62.76	6.457×10^{-4}	36.1	0.5			
Ca-smectite		151.6	1.660×10^{-13}	35	1.047×10^{-11}	23.6	0.34	3.020×10^{-17}	58.9	-0.4
Pyrite		12.9	$k_{25}=2.818 \times 10^{-5}$ $E_a =56.9$ n($O_2(aq)$)=0.5		$k_{25}=3.02 \times 10^{-8}$ $E_a =56.9$ n(H^+)=-0.5, n(Fe^{3+})=0.5					

Results and discussion

Figure 8 shows water saturations as a function of radial distance (gas CO_2 saturations are complementary to water saturations, or $S_g = 1 - S_l$). Water saturations are lower close to the CO_2 injection well. In the first 15 m water is completely displaced and removed by CO_2 gas at 100 years.
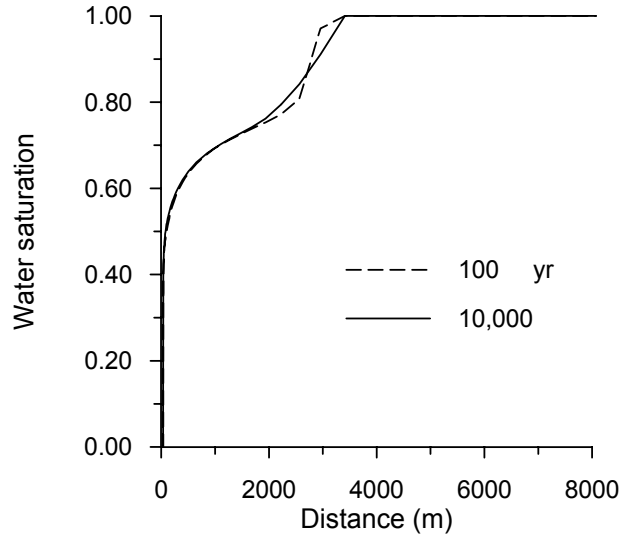
Figure 8. Water saturations at different times for the 1-D radial flow problem.

Significant ankerite and dawsonite precipitate due to CO_2 injection and dissolution of alumino-silicate minerals (Figure 9). Minor siderite and very slight magnesite precipitation occurs. No dolomite precipitation is observed in the simulation. Calcite dissolves rather than precipitates in the injected CO_2 plume region, but minor calcite precipitation occurs in background region. The cumulative sequestration of CO_2 by carbonate precipitation is given in Figure 10.

(a)

(b)
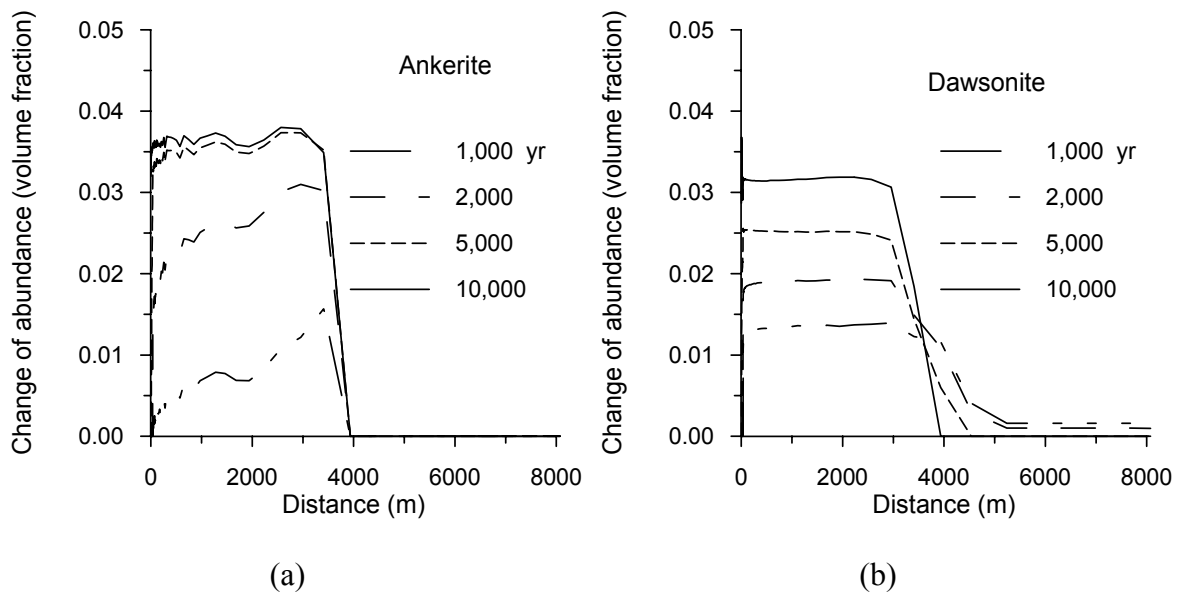
Figure 9. Change in mineral abundance (negative values indicate dissolution and positive precipitation) after different times for the 1-D radial flow problem.
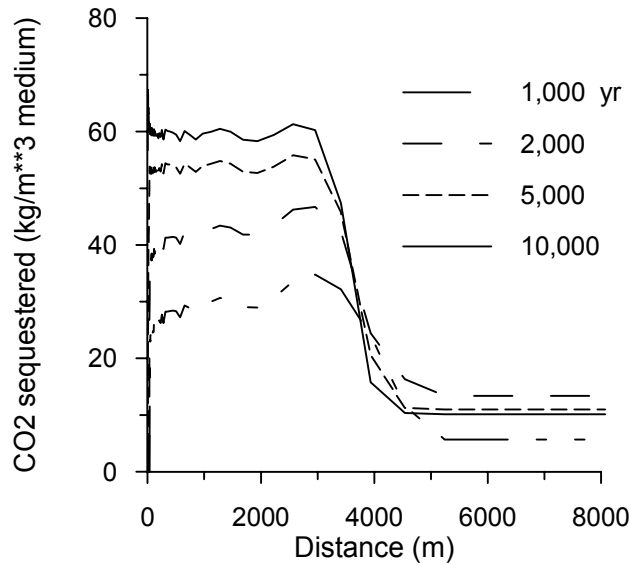
Figure 10. Cumulative CO_2 sequestration by carbonate precipitation for different times. The positive values in the background region (x > 4000 m) are due to calcite precipitation.

6. Conclusions

A non-isothermal reactive fluid flow and geochemical transport program, TOUGHREACT, has been developed by introducing reactive geochemistry into the framework of the existing widely used geothermal reservoir simulator TOUGH2. TOUGHREACT includes comprehensive chemical interactions between liquid, gaseous and solid phases that are coupled to solute transport and subsurface multiphase fluid and heat flow. The program is applicable to porous media as well as to fractured rocks. An integral finite difference (IFD) technique is employed for space discretization. The IFD methodology can deal with irregular grids, does not require reference to a global system of coordinates, and includes classical dual-continua, multiple interacting continua, and multi-region models for heterogeneous and fractured rocks as special cases. Non-isothermal effects are considered, including water-vapor phase change and air partitioning between the liquid and gas phases, temperature-dependence of

thermophysical properties such as phase density and viscosity, and chemical properties such as thermodynamic and kinetic parameters. Chemical reactions considered under the local equilibrium assumption include aqueous complexation, acid-base, redox, gas dissolution/exsolution, and cation exchange. Mineral dissolution/precipitation can proceed either subject to local equilibrium or kinetic conditions.

TOUGHREACT is applicable to one-, two-, or three-dimensional geologic domains with physical and chemical heterogeneity, and can be applied to a wide range of subsurface conditions of pressure, temperature, water saturation, ionic strength, and pH and Eh. The program can be applied to a variety of problems, including (1) contaminant transport with linear Kd adsorption and decay, (2) natural groundwater quality evolution under ambient conditions, (3) assessment of nuclear waste disposal sites, (4) sedimentary diagenesis and CO_2 disposal in deep formations, (5) mineral deposition such as supergene copper enrichment, and (6) mineral alteration and silica scaling in hydrothermal systems under natural and production conditions. Many other types of geologic, experimental, and engineered systems could be analyzed using the program.

Appendix A. Kinetic rate law for mineral dissolution and precipitation

The general rate expression used in TOUGHREACT is given by Lasaga et al. (1994) and Steefel and Lasaga (1994):

$$r_n = \pm k_n A_n \left| 1 - \left(\frac{Q_n}{K_n} \right)^\theta \right|^\eta \qquad (1)$$

where n denotes kinetic mineral index, positive values of r_n indicate dissolution, and negative values precipitation, k_n is the rate constant (moles per unit mineral surface area and unit time) which is temperature dependent, A_n is the specific reactive surface area per kg H_2O, K_n is the equilibrium constant for the mineral-water reaction written for the destruction of one mole of mineral n, and Q_n is the reaction quotient. The parameters θ and η must be determined from experiments; usually, but not always, they are taken equal to one.

For many minerals, the kinetic rate constant k can be summed from three mechanisms (Lasaga et al., 1994; Palandri and Kharaka, 2004), or

$$
k = k_{25}^{nu} \exp\left[\frac{-E_a^{nu}}{R}\left(\frac{1}{T} - \frac{1}{298.15}\right)\right] + k_{25}^{H} \exp\left[\frac{-E_a^{H}}{R}\left(\frac{1}{T} - \frac{1}{298.15}\right)\right] a_H^{n_H}
$$
$$
+ k_{25}^{OH} \exp\left[\frac{-E_a^{OH}}{R}\left(\frac{1}{T} - \frac{1}{298.15}\right)\right] a_{OH}^{n_{OH}}
$$

$$\text{(A.2)}$$

where superscripts or subscripts nu, H, and OH indicate neutral, acid and base mechanisms, respectively, E_a is the activation energy, k_{25} is the rate constant at 25°C, R is gas constant, T is absolute temperature, a is the activity of the species; and n is power term (constant). Notice that parameters θ and η (see Eq. A.1) are assumed the same for each mechanism. The rate constant k can be also dependent on other species such as Al^{3+} and Fe^{3+}. Two or more species may be involved in one mechanism. A general form of species dependent rate constants (extension of Eq. A.2) is coded in TOUGHREACT as

$$
k = k_{25}^{nu} \exp\left[\frac{-E_a^{nu}}{R}\left(\frac{1}{T} - \frac{1}{298.15}\right)\right] + \sum_i k_{25}^{i} \exp\left[\frac{-E_a^{i}}{R}\left(\frac{1}{T} - \frac{1}{298.15}\right)\right] \prod_j a_{ij}^{n_{ij}} \quad \text{(A.3)}
$$

where superscripts or subscripts i is the additional mechanism index, and j is species index involved in one mechanism that can be primary or secondary species.

TOUGHREACT considers up to five additional mechanisms and up to five species involved in each mechanism.

Appendix B. Clay swelling

Swelling clays such as smectite and illite are layered minerals made up of negatively charged mica-like sheets, which are held together by charge-balancing interlayer cations such as Ca^{2+}, Mg^{2+}, or Na^+ (de Siqueira et al., 1999). These cations adsorb water molecules, and water films form on clay surfaces. An increase of solution ionic strength causes a reduction of the thickness of the bonded water film (shrinking). When the clay is contacted by aqueous solutions of low ionic strength, the thickness will increase and clay will swell. Using smectite as an example, this process can be schematically formulated as

$$\text{smectite} + nH_2O = \text{smectite}^*[\text{smectite} \bullet (H_2O)_n] \tag{B.1}$$
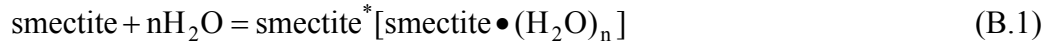
where smectite* is the swelled bulk clay with bonded water films. As water activity increases when diluting a solution of high ionic strength, the reaction (B.1) would be driven to the right. This will result in a decrease in bulk density of the clay, and consequently a reduction in porosity and permeability. The detailed mechanism of clay swelling (shrinking) is very complex. In the present study, we use a simple approach calculating the bulk clay density by

$$
\begin{aligned}
\rho &= \rho_{max}\left[1 - f_{max}\frac{I_{min} - I}{I_{min}}\right] && I < I_{min} \\
\rho &= \rho_{max} && I \geq I_{min}
\end{aligned}
\tag{B.2}
$$

where ρ_{max} is the maximum clay density achieved when ionic strength I exceeds a certain minimum value I_{min}, and f_{max} is the maximum density reduction factor when I = 0. Ionic strength I is defined as

$$I = \frac{1}{2}\sum_i c_i z_i^2 \tag{B.3}$$

where the summation is over all aqueous species, and c_i and z_i are concentration (mol/kg H_2O) and electrical charge of species i.

Appendix C. Changes of porosity and permeability

Temporal changes in porosity and permeability due to mineral dissolution and precipitation and clay swelling can modify fluid flow path characteristics. This feedback between flow and chemistry is considered in our model. Changes in porosity are calculated from changes in mineral volume fractions. Four different porosity-permeability relationships were coded in the TOUGHREACT. Here we give two relationships that were used in the two applications presented in this paper. The first one is a simple cubic Kozeny-Carman grain model:

$$\frac{k}{k_0} = \left(\frac{\phi}{\phi_0}\right)^3 \left(\frac{1-\phi_0}{1-\phi}\right)^2 \tag{C.1}$$

where ϕ is the porosity, k is the permeability (in m^2), and subscripts 0 denote initial values of variables.

Laboratory experiments have shown that modest decreases in porosity due to mineral precipitation can cause large reductions in permeability (Vaughan, 1987). This is explained by the convergent-divergent nature of natural pore channels, where pore throats can become clogged by precipitates while disconnected void spaces remain in the pore bodies. A relationship proposed by Verma and Pruess (1988), with a more sensitive coupling of permeability to porosity than the Kozeny-Carman relationship was found to better capture injectivity losses (Xu et al., 2004a):

$$\frac{k}{k_0} = \left(\frac{\phi-\phi_c}{\phi_0-\phi_c}\right)^n \tag{C.2}$$

where ϕ_c is the value of "critical" porosity at which permeability goes to zero, and n is a power law exponent. Eq. (C.2) is derived from a pore-body-and-throat model in which permeability can be reduced to zero with a finite ("critical") porosity remaining. Parameters ϕ_c and n are medium-dependent.

References

Apps, J. A., 1996. An approach to modeling of the chemistry of waste fluid disposal in deep saline aquifers, In Apps, J. A., and Tsang, C. F. (eds.). Deep injection disposal of hazardous and industrial waste: Scientific and Engineering Aspects, p. 465-488, Academic Press, San Diego, California.

Bächler, D., 2003. Coupled thermal-hydraulic-chemical modeling at the Soultz-sous-Forêts HDR reservoir (France). PhD dissertation, Swiss Federal Institute of Technology, Zurich, Switzerland.

Corey, A.T., 1954. The interrelation between gas and oil relative permeabilities, Producers Monthly, 38-41.

Durst, D., 2002. Geochemical modeling of the Soultz-sous-Forêts Hot Dry Rock test site: Coupled fluid-rock interaction to heat and fluid transport. PhD dissertation, Université de Neuchâtel, France.

de Siqueira, A.V., Lobban, C., Skipper, N.T., Williams, G.D., Soper, A.K., Done, R., Dreyer, J.W., Humphreys, R.J., Bones, J.A.R., 1999. The structure of pore fluids in swelling clays at elevated pressures and temperatures. J. Phys.: Condens. Matter 11, 9179-9188.

Dobson, P.F., Kneafsey, T.J., Sonnenthal, E.L., Spycher, N., Apps, J.A., 2003. Experimental and numerical simulation of dissolution and precipitation: implications for fracture sealing at Yucca Mountain, Nevada, Journal of Contaminant Hydrology, v. 62-63, p. 459-476.

Dobson, P.F., Salah, S., Spycher, N., Sonnenthal, E.L., 2004. Simulation of water-rock interaction in the Yellowstone geothermal system using TOUGHREACT. Geothermics, v. 33, p. 493-502.

Ennis-King, J., and Paterson, L., 2003. Role of convective mixing of the long-term storage of carbon dioxide in deep saline formations. Paper SPE 84344, Presented at Society of Petroleum Engineers Annual Fall Technical Conference and Exhibition, Denver, CO, October.

Gunter W.D., Wiwchar, B., and Perkins, E.H., 1997. Aquifer disposal of CO_2-rich greenhouse gases: extension of the time scale of experiment for CO_2-sequestering reactions by geochemical modeling. Mineral. and Petrol., v. 59, p. 121-140, 1997.

Hitchon, B. (ed.)., 1996. Aquifer Disposal of Carbon Dioxide. Geoscience Publishing, Ltd., Sherwood Park, Alberta, Canada.

Helgeson, H.C., Kirkham, D.H., Flowers, G.C., 1981. Theoretical prediction of the thermodynamic behavior of aqueous electrolytes at high pressures and temperatures: IV. Calculation of activity coefficients, osmotic coefficients, and apparent molal and standard and relative partial molal properties to 600 C and 5 kb. American Journal of Science, v. 281, p. 1249–1516.

Jacquot, E., 2000. Modéllisation thermodynamique et cinétique des reactions géochimiques entre fluids de basin et socle cristalline. Application au site experimental du programme européen de recherché en géothermie profonde (Soultz-sous-Forêts, Bas Rhin, France). PhD dissertation, Univ. Louis Pasteur, Strasbourg, France.

Johnson. J.W., Nitao, J.J., Steefel, C.I., Knaus, K.G., 2001. Reactive transport modeling of geologic CO_2 sequestration in saline aquifers: The influence of intra-aquifer shales and the relative effectiveness of structural, solubility, and mineral trapping during prograde and retrograde sequestration, In proceedings: First National Conference on Carbon Sequestration. Washington, DC, May 14-17.

Kim, J., Schwartz, F.W., Xu, T., Choi, H., Kim, I.S., 2004. Coupled processes of fluid flow, solute transport, and geochemical reactions in reactive barriers. Vadose Zone Journal, v. 3, p. 867-874.

Kiryukhin, A., Xu, T., Pruess, K., Apps, J., Slovtsov, I., 2004. Thermal-hydrodynamic-chemical (THC) modeling based on geothermal field data, Geothermics, v. 33(3), p. 349-381.

Korbol, R., Kaddour, A., 1995. Sleipner vest CO_2 disposal - injection of removed CO_2 into the Utsira Formation, Energy Convers. Mgmt., v. 36(6-9), p. 509-512.

Lasaga, A.C., Soler, J.M., Ganor, J., Burch, T.E., Nagy, K.L., 1994. Chemical weathering rate laws and global geochemical cycles. Geochimica et Cosmochimica Acta, v. 58, p. 2361-2386.

Lichtner, P.C., 1988. The quasi-stationary state approximation to coupled mass transport and fluid-rock interaction in a porous medium, Geochimica et Cosmochimica Acta, v.52, p.143-165.

Lohuis, J.A.O., 1993. Carbon dioxide disposal and sustainable development in The Netherlands, Energy Convers. Mgmt. 34(9-11), 815-821.

McPherson, B.J.O.L., Lichtner, P.C., 2001. CO_2 sequestration in deep aquifers, In proceedings: First National Conference on Carbon Sequestration. Washington, DC.

Moore, D.E., Morrow, C.A., and Byerlee, J.D., 1983. Chemical reactions accompanying fluid flow through granite held in a temperature gardient. Geochimica et Cosmochimica Acta, v. 47, p. 445-453.

Nagy, K. L., 1995. Dissolution and precipitation kinetics of sheet silicates. Chemical Weathering Rates of Silicate Minerals, v. 31, p. 291–351.

Narasimhan, T.N., Witherspoon, P.A., 1976. An integrated finite difference method for analyzing fluid flow in porous media, Water Resources Research, v. 12, p. 57–64.

Palandri, J., Kharaka, Y.K., 2004. A compilation of rate parameters of water-mineral interaction kinetics for application to geochemical modeling. US Geol. Surv. Open File Report 2004-1068, 64 pp.

Pruess, K., Narasimhan, T. N., 1985. A practical method for modeling fluid and heat flow in fractured porous media. Society of Petroleum Engineers Journal, v. 25, p. 14-26.

Pruess, K., Oldenburg, C., Moridis, G., 1999. TOUGH2 user's guide, Version 2.0. Lawrence Berkeley Laboratory Report LBL-43134, Berkeley, California, 192 pp.

Richards, L.A., 1931. Capillary conduction of liquids through porous mediums. Physics, v. 1, p. 318-333.

Simunek, J., Suares, D.L., 1994. Two-dimensional transport model for variably saturated porous media with major ion chemistry. Water Resource Research, v. 30, p. 1115-1133.

Singleton, M.J., Sonnenthal, E.L., Conrad, M.E., DePaolo, D.J., Gee, G.W., 2004. Multiphase reactive transport modeling of seasonal infiltration events and stable isotope fractionation in unsaturated zone pore water and vapor at the Hanford site. Vadose Zone Journal, v. 3, p. 775-785.

Slider, H.C., 1976. Practical petroleum reservoir engineering methods, An Energy Conservation Science. Tulsa, Oklahoma, Petroleum Publishing Company.

Sonnenthal, E., Spycher, N., 2000. Drift-scale coupled processes model. Analysis and model report (AMR) N0120/U0110, Yucca Mountain Nuclear Waste Disposal Project, Lawrence Berkeley National Laboratory, Berkeley, California.

Spycher, N.F., Sonnenthal, E.L., Apps, J.A., 2003. Fluid flow and reactive transport around potential nuclear waste emplacement tunnels at Yucca Mountain, Nevada, Journal of Contaminant Hydrology, v.62-63, p.653-673.

Steefel, C. I., 2001. CRUNCH. Lawrence Livermore National Laboratory, 76 pp.

Steefel, C.I., van Cappellen, P., 1990. A new kinetic approach to modeling water-rock interaction: The role of nucleation, precursors and Ostwald ripening. Geochimica et Cosmochimica Acta, v. 54, p. 2657-2677.

Steefel, C.I., Lasaga, A.C., 1994. A coupled model for transport of multiple chemical species and kinetic precipitation/dissolution reactions with applications to reactive flow in single phase hydrothermal system. American Journal of Science, v. 294, p. 529-592.

Steefel, C.I., MacQuarrie, K.T.B., 1996. Approaches to modeling of reactive transport in porous media, In Lichtner, P.C., Steefel, C.I., Oelkers, E.H. (eds.), Reactive transport in porous media. Reviews in Mineralogy, Mineral Society of America, v. 34, p. 83-129.

Todaka, N., Akasaka, C., Xu, T., Pruess, K., 2004. Reactive geothermal transport simulations to study the formation mechanism of an impermeable barrier between acidic and neutral fluid zones in the Onikobe Geothermal Field, Japan. Journal of Geophysical Research, v. 109, B05209, doi:10.1029/2003JB002792.

Van Genuchten, M.T., 1980. A closed-form equation for predicting the hydraulic conductivity of unsaturated soils. Soil Sci. Soc. Am. J., v. 44, p. 892-898.

Vaughan, P.J., 1987. Analysis of permeability reduction during flow of heated, aqueous fluid through Westerly Granite, in C.F. Tsang (ed.), Coupled processes associated with nuclear waste repositories, p. 529-539, Academic Press, New York.

Verma, A., Pruess, K., 1988. Thermohydrological conditions and silica redistribution near high-level nuclear wastes emplaced in saturated geological formations. Journal of Geophysical Research, v. 93, p. 1159-1173.

Vinsome, P.K.W., Westerveld, J., 1980. A simple method for predicting cap and base rock heat losses in thermal reservoir simulators. J. Canadian Pet. Tech., v. 19 (3), p. 87–90.

Walter, A.L., Frind, E.O., Blowes, D.W., Ptacek, C.J., Molson, J.W., 1994. Modeling of multicomponent reactive transport in groundwater: 1, Model development and evaluation. Water Resource Research, v. 30, p. 3137-3148.

White, S.P., 1995. Multiphase non-isothermal transport of systems of reacting chemicals. Water Resource Research, v. 31, p. 1761-1772.

White, S.P., Weir, G.J., Kissling, W.M., 2001(May 14-17). Numerical simulation of CO_2 sequestration in natural CO_2 reservoirs on the Colorado Plateau. In Proceedings of First National Conference on Carbon Sequestration, Washington, DC.

Wolery, T.J., 1992. EQ3/6: Software package for geochemical modeling of aqueous systems: Package overview and installation guide (version 8.0). Lawrence Livermore National Laboratory Report UCRL-MA-110662 PT I, Livermore, California.

Xu, T., Pruess, K., 1998. Coupled modeling of non-isothermal multiphase flow, solute transport and reactive chemistry in porous and fractured media: 1. Model development and validation. Lawrence Berkeley National Laboratory Report LBNL-42050, Berkeley, California, 38 pp.

Xu, T., Pruess, K., Brimhall, G., 1999a. An improved equilibrium-kinetics speciation algorithm for redox reactions in variably saturated flow systems. Computers & Geosciences, v.25(6), p. 655-666.

Xu, T., Samper, J., Ayora, C., Manzano, M., and Custodio, E., 1999b. Modeling of non-isothermal multi-component reactive transport in field-scale porous media flow system. Journal of Hydrology, v. 214, p. 144-164.

Xu, T., White, S.P., Pruess, K., Brimhall, G. H., Apps, J., 2000. Modeling of pyrite oxidation in saturated and unsaturated subsurface flow systems. Transport in Porous Media, v. 39, p. 25-56.

Xu, T., Pruess, K., 2001a. On fluid flow and mineral alteration in fractured caprock of magmatic hydrothermal systems. Journal of Geophysical Research, v. 106 (B2), p. 2121-2138.

Xu, T., Pruess, K., 2001b. Modeling multiphase non-isothermal fluid flow and reactive geochemical transport in variably saturated fractured rocks: 1. Methodology. American Journal of Science, v. 301, p. 16-33.

Xu, T., Sonnenthal, E., Spycher, N., Pruess, K., Brimhall, G., Apps, J., 2001. Modeling multiphase non-isothermal fluid flow and reactive geochemical transport in variably saturated fractured rocks: 2. Applications to supergene copper enrichment and hydrothermal flows. American Journal of Science, v. 301, p. 34-59.

Xu, T, Apps, J.A., Pruess, K., 2003a. Reactive geochemical transport simulation to study mineral trapping for CO_2 disposal in deep arenaceous formations. Journal of Geophysical Research, v. 108(B2), 2071, doi:10.1029/2002JB001979.

Xu, T., Sonnenthal, E., Bodvarsson, G., 2003b. A reaction-transport model for calcite precipitation and evaluation of infiltration fluxes in unsaturated fractured rock. Journal of Contaminant Hydrology, v. 64(1-2) p. 113 - 127.

Xu, T., Ontoy, Y., Molling, P., Spycher, N., Parini, M., Pruess, K., 2004a. Reactive transport modeling of injection well scaling and acidizing at Tiwi Field, Philippines. Geothermics, v. 33(4), p. 477-491.

Xu, T, Apps, J.A., Pruess, K., 2004b. Numerical simulation to study mineral trapping for CO2 disposal in deep aquifers. Applied Geochemistry, v. 19, p. 917-936.

Xu, T., Sonnenthal, E., Spycher, N., Pruess, K., 2004c. TOUGHREACT user's guide: A simulation program for non-isothermal multiphase reactive geochemical transport in variable saturated geologic media. Lawrence Berkeley National Laboratory Report LBNL-55460, Berkeley, California, 192 pp.

Yeh, G.T., Tripathi, V.S., 1991. A model for simulating transport of reactive multispecies components: model development and demonstration. Water Resource Research, v. 27, p. 3075-3094.